Vol.3 pp. 32-39 International Journal of Renewable Energy and Sustainability (RES)

Field Oriented Control of a Dual Star Induction Machine Fed by Photovoltaic Solar Panel with MPPT

SADOUNI Radhwane[#1], MEROUFEL Abdelkader[#2], DJERIOU Salim[*3] KHALDOUNE Aissa[*4]

[#] *Sciences and Technics Department,University of Ghardaia, Algeria.*

[#] *ICEPS laboratory, Djillali Liabes University, SBA, Algeria.*

[1]redouanesadouni@gmail.com

[2]ameroufel@yahoo.fr

[*] *Signals and systems laboratory, IGEE, Boumerdes, Algeria.*

[3]Salimjr28@yahoo.fr

[4]akheldoun@umbb.dz

***Abstract*— This paper presents a maximum power point tracking (MPPT) applied to Dual Star Induction Machine supplied by photovoltaic solar panel. The indirect field oriented control with PI speed controller is used for the control of this machine fed by two PWM voltage source inverter. The simulation results using Matlab/Simulink environment prove the efficiency of the proposed method.**

***Keywords*—** Photovoltaic Generator; DSIM; PWM-VSI; Indirect Field Oriented Control; PI Controller.

I. INTRODUCTION

Electrical energy results from the transformation of natural fossil resources. However, this transformation is accompanied with an emission of polluting gas. In this way, production of electricity via renewable energies becomes more and more employed in order to vouch for protection of environment and durable development.

Photovoltaic energy is a renewable energy source, inexhaustible and non-polluting. To be used for different applications and to meet the economic constraints, the design and implementation of PV systems are necessary and currently facing many problems. The PV system must be made robust, reliable and with high efficiency [1].

In the industrial applications that high reliability is demanded, multi-phase induction machine instead of traditional three-phase induction machine is used. The advantages of multi-phase drive systems over conventional three-phase drives are: total rating of system is multiplied, the torque pulsations will be smoothed, the rotor harmonic losses as well as the harmonics content of the DC link current will be reduced and the loss of one machine phase, does not prevent the machine working, so improving the system reliability [2]. A common type of multiphase machine is the dual star induction machine (DSIM), is also known as the six phase induction machine, these machines have been used in many applications (water pumping system, fans, compressors, rolling mills, cement mills, mine hoists…etc.) for their advantages in power segmentation, reliability, and minimized torque pulsations [3].

Field Oriented Control (FOC) is theoretically a nonlinear control technique that linearizes the complex dynamics of the induction motor. Rotor flux indirect FOC, which is the more simplest decoupling scheme, is widely used in many industrial applications [4].

The Indirect Rotor Field Oriented Control (IRFOC) with PI speed regulator for the Dual Star Induction Machine fed by MPPT photovoltaic generator is elaborate in this work.

II. SYSTEM MODELING

The figure 1 shows the proposed structure of the MPPT photovoltaic generator fed the DSIM using direct rotor field oriented control.

A. Modeling of the photovoltaic generator PVG

The direct conversion of the solar energy into electrical power is obtained by solar cells [7]. The cells are connected in series and in parallel combinations in order to form an array of the desired voltage and power levels. The figure 2 shows the equivalent circuit of a PVG, from which non linear I–V characteristic can be deduced [1], [8], [9].

ISSN: 2961-6603

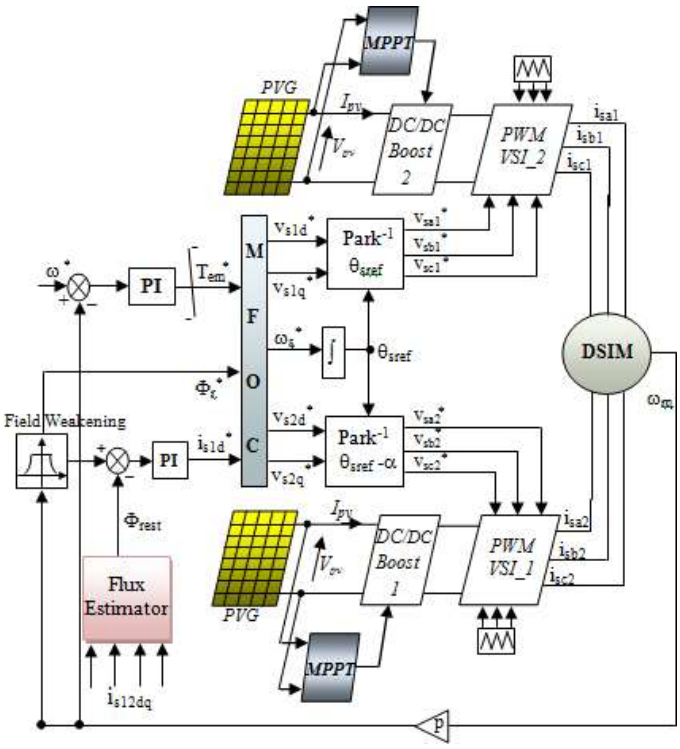

Fig. 1 Direct method speed regulation of DSIM fed by PVG with MPPT

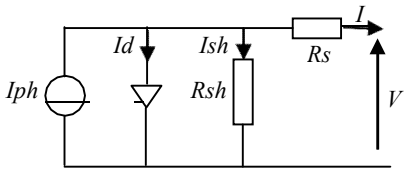

Fig. 2 Equivalent circuit of a PV module

$$I = I_{ph} - I_d - I_{sh} \quad (1)$$

$$I_d = I_0\left(e^{\left(\frac{q(V+R_s I)}{kAT}\right)} - 1\right) \quad (2)$$

$$I_{sh} = \frac{V + R_s I}{R_{sh}} \quad (3)$$

Where:
I_{ph}: is the photocurrent
I_d: is the junction diode current
I_0: is the reverse saturation current
R_s: is the series resistance
R_{sh}: is the parallel resistance
A: is the diode factor
k: is the Boltzmann's constant
T: is the cell temperature
q: is the electron charge

The figure 3 represents the experiment characteristics of P-V and I-V characteristics of the solar-cell generator for several insulation levels.

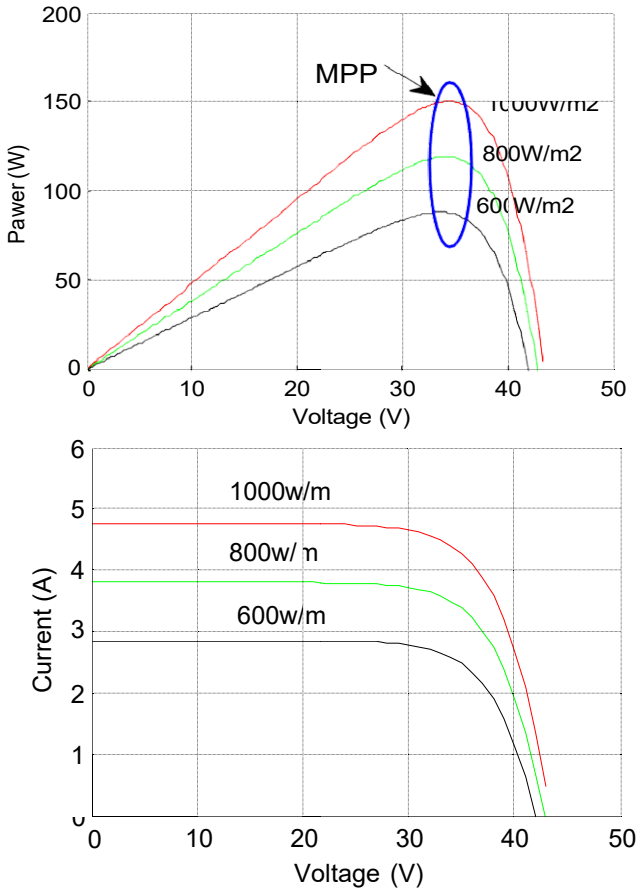

Fig. 3 Influence of radiation

B. Modeling of the DC-DC Boost Converter

To extract at each moment the maximum power available at the terminals of the PV and transfer it to the load, the technique conventionally used is to use a stage adaptation between the PV and the load. In our study we use a boost converter, as voltages elevators, are also used in photovoltaic applications, especially in photovoltaic pumping system.

This converter plays the role of an interface between the two elements ensuring through control action, the transfer of maximum power supplied by the generator to make it as close as possible to PMAX.

MPPT is the maximum power point tracking which is essential for optimizing the array operation and the system performance. Several techniques have been proposed to achieve this goal, among them we can mention perturb and observe and incremental conductance [10]. Figure 4 shows the flowchart of this algorithm.

ISSN: 2961-6603

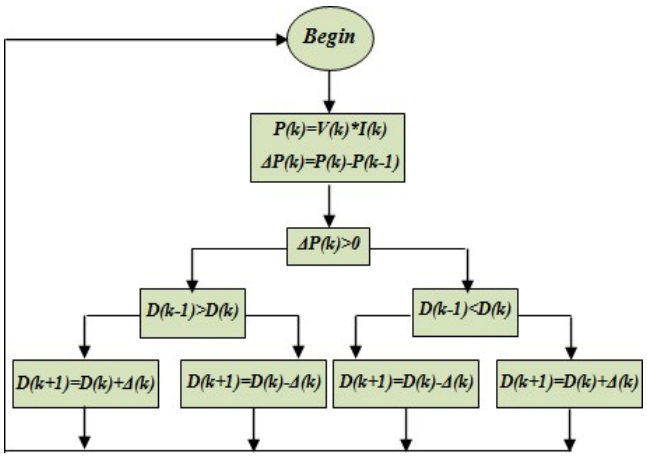

Fig. 4 Flowchart of the P&O algorithm

C. Modeling of the PWM Voltage Source Inverter

The three-phase inverter consists of three independent arms. Each one includes two switches which are complementary and controlled by the Pulse Width Modulation PWM, [11], [12]. The induction motor stator voltages (V_{sa}, V_{sb}, V_{sc}) are expressed in terms of the upper switches as follows:

$$\begin{bmatrix} V_{sa} \\ V_{sb} \\ V_{sc} \end{bmatrix} = \frac{U_{pv}}{3} \begin{bmatrix} 2 & -1 & -1 \\ -1 & 2 & -1 \\ -1 & -1 & 2 \end{bmatrix} \begin{bmatrix} f_{11} \\ f_{12} \\ f_{13} \end{bmatrix} \quad (4)$$

U_{pv}: The photovoltaic voltage

f_{11}, f_{12} and f_{13} are the controller signals applied to the switches. Figure 5 shows the flowchart of these signals.

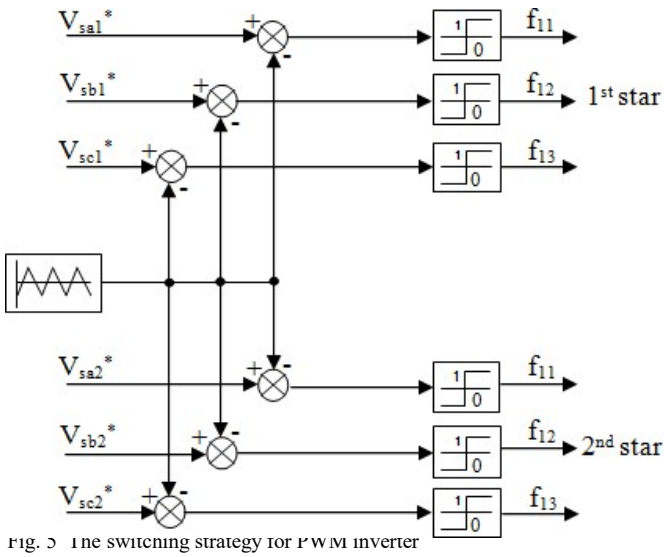

Fig. 5 The switching strategy for PWM inverter

D. Modeling of the DSIM

A schematic of the stator and rotor windings for a dual star induction machine is given in Figure 6. The six stator phases are divided into two wyes-connected three phase sets labelled A_{s1}, B_{s1}, C_{s1} and A_{s2}, B_{s2}, C_{s2} whose magnetic axes are displaced by an angle α=30°. The windings of each three phase set are uniformly distributed and have axes that are displaced 120° apart. The three phase rotor windings A_r, B_r, C_r are also sinusoidally distributed and have axes that are displaced apart by 120° [13].

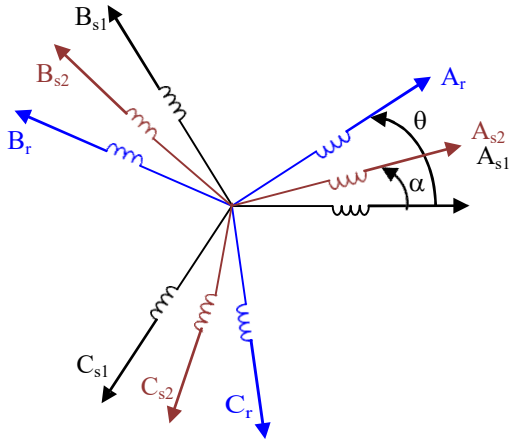

Fig. 6 Windings of the dual star induction machine

The voltage equations of the DSIM are as follow [14]:

$$[V_{s1}] = \begin{bmatrix} V_{sa1} \\ V_{sb1} \\ V_{sc1} \end{bmatrix} = [R_{s1}][I_{s1}] + \frac{d}{dt}[\Phi_{s1}]$$

$$[V_{s2}] = \begin{bmatrix} V_{sa2} \\ V_{sb2} \\ V_{sc2} \end{bmatrix} = [R_{s2}][I_{s2}] + \frac{d}{dt}[\Phi_{s2}] \quad (5)$$

$$[0] = \begin{bmatrix} V_{ra} \\ V_{rb} \\ V_{rc} \end{bmatrix} = [Rr][Ir] + \frac{d}{dt}[\Phi_r]$$

Where:

$R_{sa1} = R_{sb1} = R_{sc1} = R_{s1}$: Star resistance 1.

$R_{sa2} = R_{sb2} = R_{sc2} = R_{s2}$: Star resistance 2.

$R_{ra} = R_{rb} = R_{rc} = R_r$: Rotor resistance.

$$[R_{s1}] = \begin{bmatrix} R_{s1} & 0 & 0 \\ 0 & R_{s1} & 0 \\ 0 & 0 & R_{s1} \end{bmatrix}; [R_{s2}] = \begin{bmatrix} R_{s2} & 0 & 0 \\ 0 & R_{s2} & 0 \\ 0 & 0 & R_{s2} \end{bmatrix}; [R_r] = \begin{bmatrix} R_r & 0 & 0 \\ 0 & R_r & 0 \\ 0 & 0 & R_r \end{bmatrix} \quad (6)$$

$$[I_{s1}] = \begin{bmatrix} I_{sa1} \\ I_{sb1} \\ I_{sc1} \end{bmatrix}; [I_{s2}] = \begin{bmatrix} I_{sa2} \\ I_{sb2} \\ I_{sc2} \end{bmatrix}; [I_r] = \begin{bmatrix} I_{ra} \\ I_{rb} \\ I_{rc} \end{bmatrix} \quad (7)$$

ISSN: 2961-6603

$$[\Phi_{s1}]=\begin{bmatrix}\Phi_{sa1}\\ \Phi_{sb1}\\ \Phi_{sc1}\end{bmatrix};[\Phi_{s2}]=\begin{bmatrix}\Phi_{sa2}\\ \Phi_{sb2}\\ \Phi_{sc2}\end{bmatrix};[\Phi_{r}]=\begin{bmatrix}\Phi_{ra}\\ \Phi_{rb}\\ \Phi_{rc}\end{bmatrix} \quad (8)$$

The expressions for star and rotor flux are [14]:

$$\begin{bmatrix}[\Phi_{s1}]\\ [\Phi_{s2}]\\ [\Phi_{r}]\end{bmatrix}=\begin{bmatrix}[L_{s1s1}] & [L_{s1s2}] & [L_{s1r}]\\ [L_{s2s1}] & [L_{s2s2}] & [L_{s2r}]\\ [L_{rs1}] & [L_{rs2}] & [L_{rr}]\end{bmatrix}\begin{bmatrix}[I_{s1}]\\ [I_{s2}]\\ [I_{r}]\end{bmatrix} \quad (9)$$

Where:

$[L_{s1s1}]$: Inductance matrix of the star 1.
$[L_{s2s2}]$: Inductance matrix of the star 2.
$[L_{rr}]$: Inductance matrix of the rotor.
$[L_{s1s2}]$: Mutual inductance matrix between star 1 and star 2.
$[L_{s2s1}]$: Mutual inductance matrix between star 2 and star 1.
$[L_{s1r}]$: Mutual inductance matrix between star 1 and rotor.
$[L_{s2r}]$: Mutual inductance matrix between star 2 and rotor.
$[L_{rs1}]$: Mutual inductance matrix between rotor and star 1.
$[L_{rs2}]$: Mutual inductance matrix between rotor and star 2.

The expression of the electromagnetic torque is then as follows [14], [15], [16]:

$$Tem=\left(\frac{p}{2}\right)\left([I_{s1}]^{t}\frac{d}{d\theta}[L_{s1r}][I_{r}]+[I_{s2}]^{t}\frac{d}{d\theta}[L_{s2r}][I_{r}]\right) \quad (10)$$

The Park model of the DSIM in the references frame at the rotating field (*d, q*), is defined by the following equations system (11) [17].

The figure 7 represents the model of the DSIM in the Park frame.

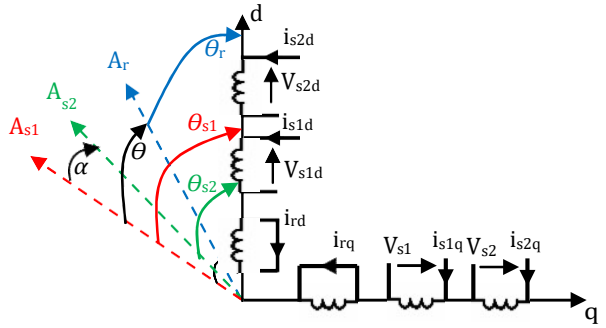

Fig. 7 Representation of DSIM in the Park frame

$$\begin{aligned}
V_{s1d}&=R_{s1}I_{s1d}+\frac{d}{dt}\Phi_{s1d}-\omega_s\Phi_{s1q}\\
V_{s1q}&=R_{s1}I_{s1q}+\frac{d}{dt}\Phi_{s1q}+\omega_s\Phi_{s1d}\\
V_{s2d}&=R_{s2}I_{s2d}+\frac{d}{dt}\Phi_{s2d}-\omega_s\Phi_{s2q}\\
V_{s2q}&=R_{s2}I_{s2q}+\frac{d}{dt}\Phi_{s2q}+\omega_s\Phi_{s2d}\\
0&=R_rI_{rd}+\frac{d\Phi_{rd}}{dt}-\omega_{sr}\Phi_{rq}\\
0&=R_rI_{rq}+\frac{d\Phi_{rq}}{dt}+\omega_{sr}\Phi_{rd}
\end{aligned} \quad (11)$$

Where:

$$\begin{aligned}
\Phi_{s1d}&=L_{s1}I_{s1d}+L_m(I_{s1d}+I_{s2d}+I_{rd})\\
\Phi_{s1q}&=L_{s1}I_{s1q}+L_m(I_{s1q}+I_{s2q}+I_{rq})\\
\Phi_{s2d}&=L_{s2}I_{s2d}+L_m(I_{s1d}+I_{s2d}+I_{rd})\\
\Phi_{s2q}&=L_{s2}I_{s2q}+L_m(I_{s1q}+I_{s2q}+I_{rq})\\
\Phi_{rd}&=L_rI_{rd}+L_m(I_{s1d}+I_{s2d}+I_{rd})\\
\Phi_{rq}&=L_rI_{rq}+L_m(I_{s1q}+I_{s2q}+I_{rq})
\end{aligned} \quad (12)$$

L_m: Cyclic mutual inductance between star 1, star 2 and rotor.

The mechanical equation is given by:

$$J\frac{d\Omega}{dt}=T_{em}-T_L-F_r\Omega \quad (13)$$

With:

$$Tem=p\frac{L_m}{L_r+L_m}\left[\Phi_{rd}(I_{s1q}+I_{s2q})-\Phi_{rq}(I_{s1d}+I_{s2d})\right] \quad (14)$$

E. Field Oriented Control

The objective of space vector control is to assimilate the operating mode of the asynchronous machine at the one of a DC machine with separated excitation, by decoupling the torque and the flux control. The IRFOC consists in making $\Phi_{qr}=0$ while the rotor direct flux Φ_{dr} converges to the reference Φ_r^* [16, 17].

By applying this principle ($\Phi_{rq}=0$ and $\Phi_{rd}=\Phi_r^*$) to equations (11) (12) and (14), the finals expressions of the electromagnetic torque and slip speed are:

$$T_{em}=p\frac{L_m}{L_m+L_r}\Phi_r^*(I_{s1q}^*+I_{s2q}^*) \quad (15)$$

$$w_{sr}^*=\frac{R_rL_m}{(L_m+L_r)\Phi_r^*}(I_{s1q}^*+I_{s2q}^*) \quad (16)$$

The stators voltage equations are:

$$\begin{cases}
V_{s1d}^*=R_{s1}I_{s1d}+L_{s1}\frac{d}{dt}I_{s1d}-\omega_s^*(L_{s1}I_{s1q}+T_r\Phi_r^*w_{sr}^*)\\
V_{s1q}^*=R_{s1}I_{s1q}+L_{s1}\frac{d}{dt}I_{s1q}+\omega_s^*(L_{s1}I_{s1d}+\Phi_r^*)\\
V_{s2d}^*=R_{s2}I_{s2d}+L_{s2}\frac{d}{dt}I_{s2d}-\omega_s^*(L_{s2}I_{s2q}+T_r\Phi_r^*w_{sr}^*)\\
V_{s2q}^*=R_{s2}I_{s2q}+L_{s2}\frac{d}{dt}I_{s2q}+\omega_s^*(L_{s2}I_{s2d}+\Phi_r^*)
\end{cases} \quad (17)$$

The torque expression shows that the reference fluxes and stator currents in quadrate are not perfectly independents, for this, it is necessary to decouple torque

ISSN: 2961-6603

and flux control of this machine by introducing new variables:

$$\begin{cases} V_{s1d} = R_{s1}I_{s1d} + L_{s1}\dfrac{d}{dt}I_{s1d} \\ V_{s1q} = R_{s1}I_{s1q} + L_{s1}\dfrac{d}{dt}I_{s1q} \\ V_{s2d} = R_{s2}I_{s2d} + L_{s2}\dfrac{d}{dt}I_{s2d} \\ V_{s2q} = R_{s2}I_{s2q} + L_{s2}\dfrac{d}{dt}I_{s2q} \end{cases} \quad (18)$$

The equation system (18) shows that stator voltages (V_{s1d}, V_{s1q}, V_{s2d}, V_{s2q}) are directly related to stator currents (I_{s1d}, I_{s1q}, I_{s2d}, I_{s2q}). To compensate the error introduced at decoupling time, the voltage references (V_{s1d}^*, V_{s2d}^*, V_{s1q}^*, V_{s2q}^*) at constant flux are given by:

$$\begin{cases} V_{s1d}^* = V_{s1d} - V_{s1dc} \\ V_{s1q}^* = V_{s1q} + V_{s1qc} \\ V_{s2d}^* = V_{s2d} - V_{s2dc} \\ V_{s2q}^* = V_{s2q} + V_{s2qc} \end{cases} \quad (19)$$

With:

$$\begin{cases} V_{s1dc} = \omega_s^* (L_{s1}I_{s1q} + T_r \Phi_r^* w_{sr}^*) \\ V_{s1qc} = \omega_s^* (L_{s1}I_{s1d} + \Phi_r^*) \\ V_{s2dc} = \omega_s^* (L_{s2}I_{s2q} + T_r \Phi_r^* w_{sr}^*) \\ V_{s2qc} = \omega_s^* (L_{s2}I_{s2d} + \Phi_r^*) \end{cases} \quad (20)$$

For a perfect decoupling, we add stator currents regulation loops (I_{s1d}, I_{s1q}, I_{s2d}, I_{s2q}) and we obtain at their output stator voltages (V_{s1d}, V_{s1q}, V_{s2d}, V_{s2q}).The decoupling bloc scheme in voltage modified (Modified Field Oriented Control) is given in Figure 8.

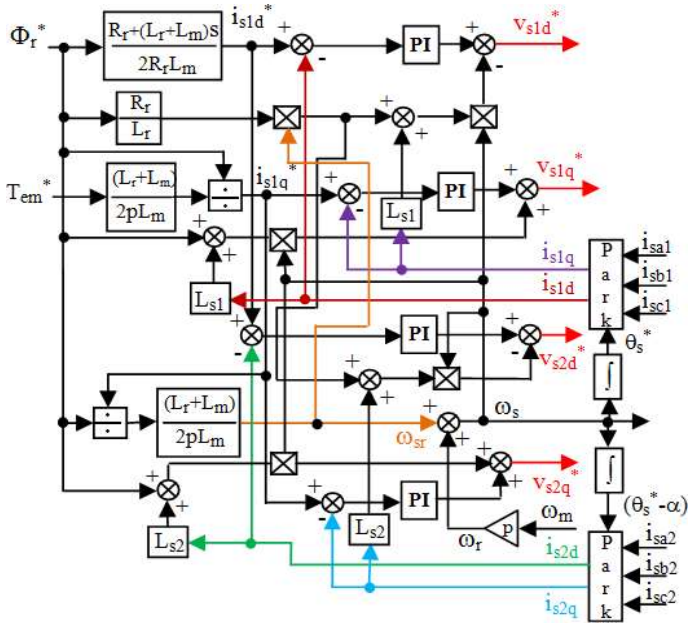

Fig. 8: decoupling bloc in voltage

III. Simulation Results

In order to demonstrate the robustness and the efficiency of the proposed scheme applied to the DTPIM using photovoltaic system, some simulations have been carried out. The design which is described by Figure 1 is implemented in Matlab/Simulink using parameters given in appendix.

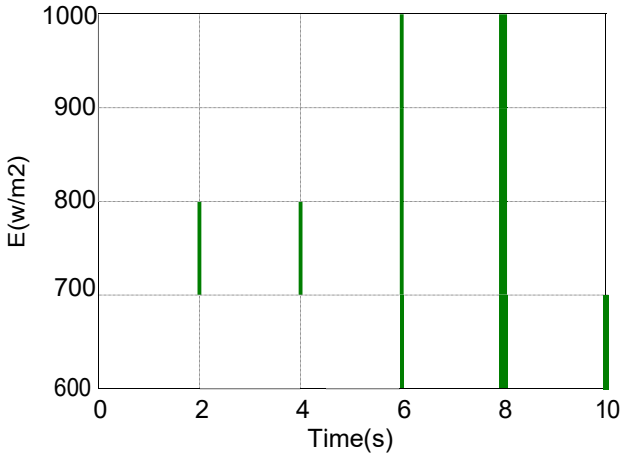

Fig.9 : Solar irradiation

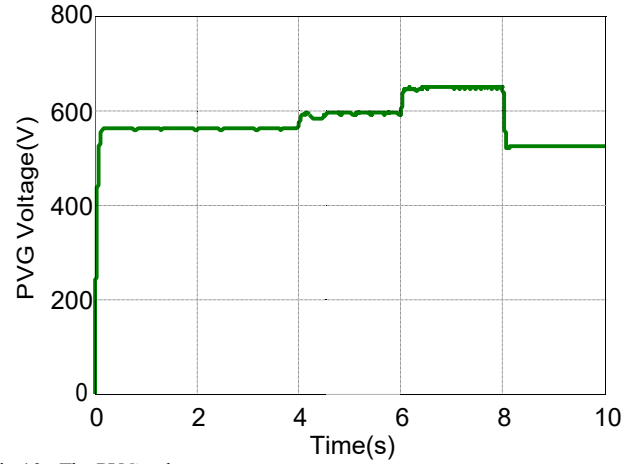

Fig.10 : The PVG voltage

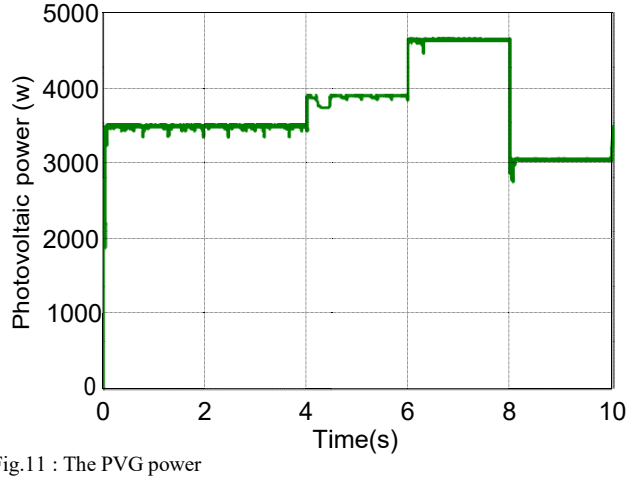

Fig.11 : The PVG power

ISSN: 2961-6603

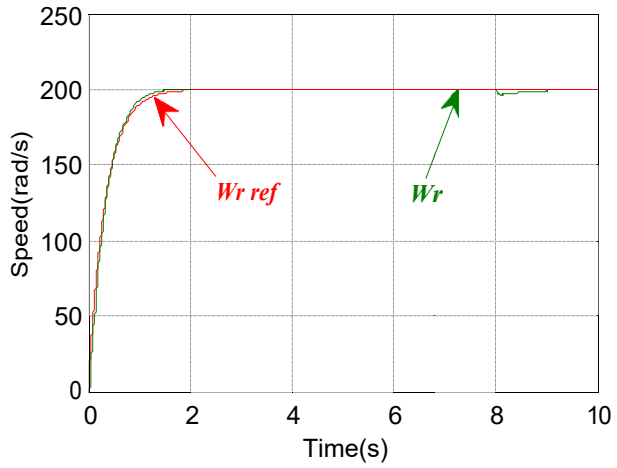

Fig.12: Rotational and reference speed

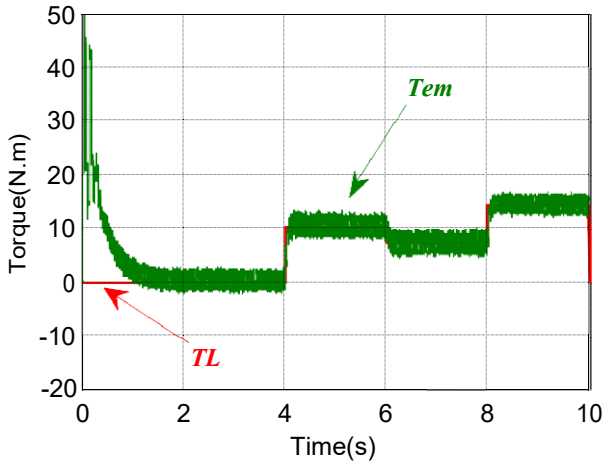

Fig.13: Electromagnetic and load torque

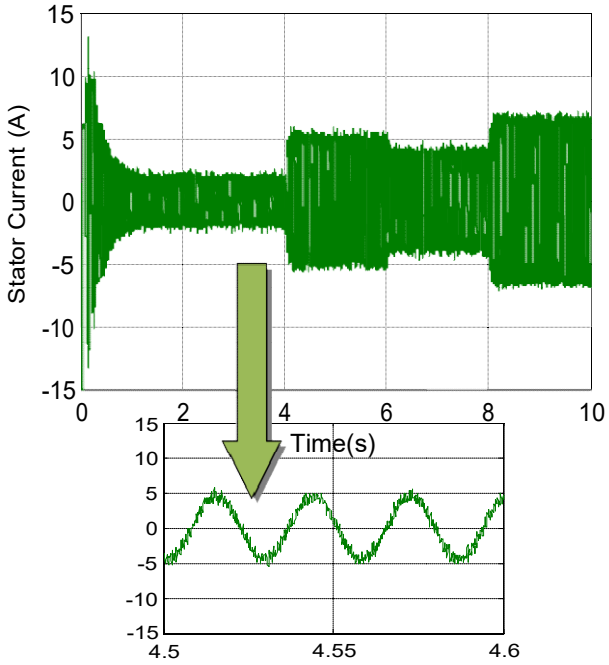

Fig.14: The stator current i_{sa1}

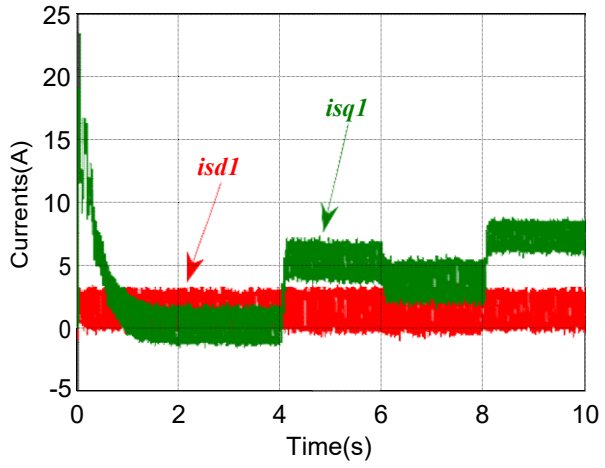

Fig.15: Decoupling between field and torque

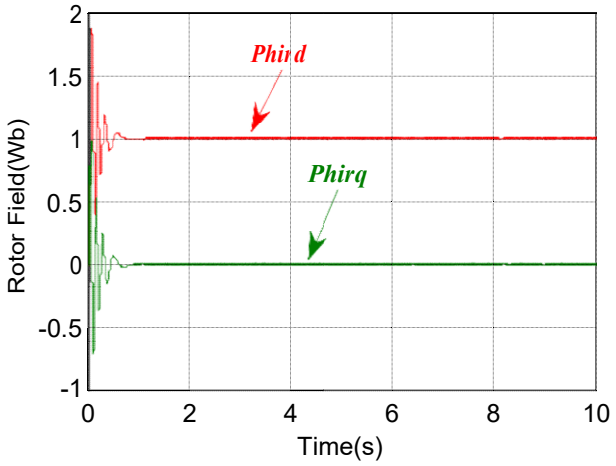

Fig.16: Rotor field orientation

IV. Results Discussion

We chose to vary the irradiation E between 700W/m^2, 800W/m^2, 1000W/m^2 and 600W/m^2 (Fig.9), the voltage and the power of photovoltaic generator are varied with the variation of irradiation (Fig.10, Fig.11).

The speed reaches its reference values without overtaking (Fig.12). The machine develops an electromagnetic torque to compensate the load torque by calling of stator current (Fig.13, Fig.14).

The electrical part (the current i_{sd1}) is insensitive to the load torque variation, only the mechanical part (the current i_{sq1}), will react (Fig.15). So, we can say that there is a good decoupling.

The direct rotor field *(Phird)* follows the reference value *(1Wb)* and the quadrature component *(Phirq)* is null (Fig.16). Thus, the orientation is assured.

ISSN: 2961-6603

V. Conclusion

In this paper, the indirect field oriented control of dual star induction machine with photovoltaic generator using MPPT is presented.

The simulation results prove the efficiency and the utility of the MPPT algorithm to make the system operates at its optimal conditions, by maintenance of the power at its maximum value with each value of irradiation E, whatever the climatic conditions.

The simulation results show the robustness, the effectiveness and the good dynamic performances (speed response without overshoot, zero state error,…etc) of IRFOC with PI regulator.

References

[1] A. Khiareddine, C. Ben Salah and M. F. Mimouni, *Control water level of a photovoltaic pumping. IEEE*, 2013.

[2] R.Kianinezhad.R, B. Nahid, F. Betin, and G. A. Capolino. A novel Direct Torque Control (DTC) method for dual three phase induction motors. *IEEE*, 2006.

[3] Y. Zhao, T. A. Lipo. Space vector PWM control of dual three phase induction machine using vector space decomposition. *IEEE Trans. Ind. Appl*, vol. 31, no. 5, pp. 1100–1109.

[4] A. BA-Razzouk, A. Chériti, G. Olivier, P. Sicard. Field Oriented Control of Induction Motors Using Neural Networks Decouplers. *IEEE*, 1995.

[5] K. Benlarbi. A fuzzy global efficiency optimization of a photovoltaic water pumping system. *Solar Energy,* 77 (2004) 203–216.

[6] A. Chikh. Optimization and Control of a Photovoltaic Powered Water Pumping System. *IEEE Electrical Power & Energy Conference*, 2009.

[7] S. Abouda. Direct torque control of induction motor pumping system fed by a photovoltaic generator. *IEEE*, 2013.

[8] S. Dezso. Optimized Maximum Power Point Tracker for Fast-Changing Environmental Conditions. *IEEE Transactions On Industrial Electronics*, vol. 55, no. 7, July 2008.

[9] Y. Weslati, A. Sallemi, F. Bacha, and R. Andoulsi. Sliding mode control of a photovoltaic grid connected system.*Journal of Electrical Systems*, vol. 4, issue 3, September 2008.

[10] Faouzi Bacha and Moncef Gasmi. Sliding Mode Control of Induction-Motor-Pump Supplied by Photovoltaic Generator. *IEEE*, 2011.

[11] G. K. Singh, K. Nam and S. K. Lim. A simple indirect field-oriented control scheme for multiphase induction machine. *IEEE Trans. Ind. Elect*, vol. 52, no. 4, August 2005.

[12] E.M. Berkouk, S. Arezki. Modélisation et Commande d'une Machine Asynchrone Double Etoile (MASDE) Alimentée par Deux Onduleurs à Cinq Niveaux à Structure NPC, *Conférence national sur le génie électrique, CNGE, Tiaret, Algérie*, 2004.

[13] A.Igoudjil ; Y.Boudjema. Etude du changeur de fréquence à cinq niveaux à cellules imbriquées. Application à la conduite de la machine Asynchrone à Double Etoile. *Mémoire d'ingéniorat de l'USTHB d'Alger, Algérie,* Juin 2006.

[14] D. Hadiouche. Contribution à l'étude de la machine asynchrone double étoile modélisation, alimentation et structure, Thèse de doctorat, Université Henri Poincaré, Nancy-1, Décembre 2001.

[15] Z.Chen, AC.Williamson. Simulation Study of a Double Three Phase Electric Machine, *International conference on Electric Machine ICEM'98*, 1998.

[16] E.Merabet, R.Abdessemed, H.Amimeur and F.Hamoudi. Field Oriented Control of a Dual Star Induction Machine Using Fuzzy Regulators, *CIP*, Sétif, Algérie, 2007.

[17] R. N. Andriamalala, H. Razik and F.M. Sargos. Indirect-Rotor-Field-Oriented-Control of a Double-Star Induction Machine Using the RST Controller, *IEEE*, 2008.

Appendix

TABLE I
Dual Star Induction Machine parameters

P_n [kw]	4.5	R_r [Ω]	2 .12	J [kg.m²]	0.0625
V_n [V]	220	L_{s1} [H]	0.022	K_f [Nms/rd]	0.001
I_n [A]	6.5	L_{s2} [H]	0.022	f [Hz]	50
R_{s1} [Ω]	3.72	L_r [H]	0.006	p	1
R_{s2} [Ω]	3.72	L_m [H]	0.367	Cos φ	0.8

TABLE II
Photovoltaic model characteristics

Electrical Characteristics	
Maximum Power (Pmax)	*150W*
Voltage at Pmax (Vmp)	*34.5V*
Current at Pmax (Imp)	*4.35A*
Open-circuit voltage (Voc)	*43.5*
Short-circuit current (Isc)	*4.75A*
Temperature coefficient of Voc	*-160 ± 20 mV/°C*
Temperature coefficient of Isc	*0.065 ± 0.015 %/°C*
Temperature coefficient of power	*-0.5 ± 0.05 %/°C*

ISSN: 2961-6603